ACS OMEGA

Open Access

http://pubs.acs.org/journal/acsodf

Article

Nanostructured SnO_2 Thin Films Based on a Convenient Chemical Deposition for Sensitive Detection of Ethanol

Yu Zhang, Quan Xie,* Lin Lyu, Jiang Zou, and Zhou Lu

Cite This: *ACS Omega* 2024, 9, 16055−16062

Read Online

ACCESS | Metrics & More | Article Recommendations | Supporting Information

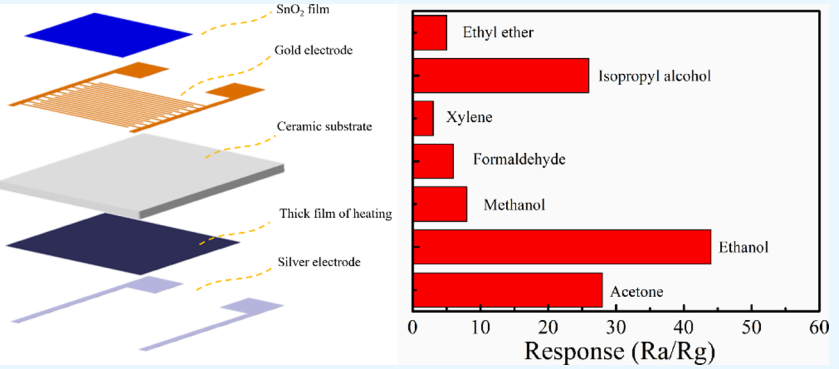

ABSTRACT: A specific matrix sensor that can operate at low temperatures and has a high sensing response is crucial for monitoring flammable VOC gases. In this study, a nanostructured SnO_2 thin film was successfully produced using a suitable chemical deposition method, and its sensing properties were comprehensively analyzed. The SEM images revealed that the thin film of the nanostructured SnO_2 is made up of two different sizes of broccoli-like structure nanoparticles. The sensor, which is based on this unique micronano structure, demonstrated a high sensing response (44), low operating temperature (200 °C), and fast response time (6s). Additionally, the nanostructured sensor exhibited excellent resistance to humidity interference and long-term stability. Moreover, DFT is employed to evaluate the electronic properties and to systematically explain the gas sensing mechanism of the nanostructured sensor based on the SnO_2 thin film.

1. INTRODUCTION

Continuous progress in the chemical industry and diverse product needs have forced us to adopt a sustainable and reliable approach to monitoring volatile organic compounds (VOCs) in the environment. According to previous research works, metal oxide semiconductors have developed an important part due to their stable chemical nature, simple structure, low operating temperature, higher sensitivity, and lower cost, for instance, SnO_2,[1−4] CeO_2,[5−8] CuO,[9,10] ZnO,[11] NiO,[12] WO_3,[13−15] Fe_2O_3,[16] and TiO_2.[17,18] Furthermore, some studies have also shown that the sensors based on oxides and sulfides still have a better sensing response even at room temperature.[17−20] The primary sensing mechanism of these semiconductor sensors is essentially attributed to the change in the width of the space charge region and subsequently the height of the potential barrier when the target gas is adsorbed on the sensor surface.[21,22]

Among the metal oxides described above, SnO_2 is a wide-bandgap n-type semiconductor (E_g = 3.6 eV at 300 K)[23] and is extensively utilized as a base material for monitoring abnormal VOC concentrations due to the chemical stability, non-stoichiometry, high electrical conductivity, and microstructure morphology being controllable.[24,25] Researchers have prepared several newly structured SnO_2 nanoparticles with a higher sensing performance by continuously exploring the gas-sensing mechanism, such as hollow nanocubes with well-aligned rod-like building blocks, which show improved sensory performance toward *n*-butanol.[26] Porous SnO_2 microcubes exhibited higher sensing response for toluene and lower operating temperature.[23] Single-crystalline tin oxide nanowires (NWs) provide a good linear response for NO_2 through thermal chemical vapor deposition.[27] Furthermore, other micro-structured nanoparticles,[28,29] nanobelts,[30] and polycrystalline nanotubes[31] exhibit relatively superior sensing properties compared to SnO_2 film sensors obtained by magnetron sputtering. Although the nanoparticles of the new structures mentioned above have substantially improved the sensing response of VOCs, the reproducibility and compatibility of the

Received: December 2, 2023
Revised: March 13, 2024
Accepted: March 18, 2024
Published: March 29, 2024

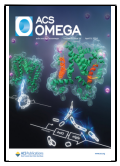

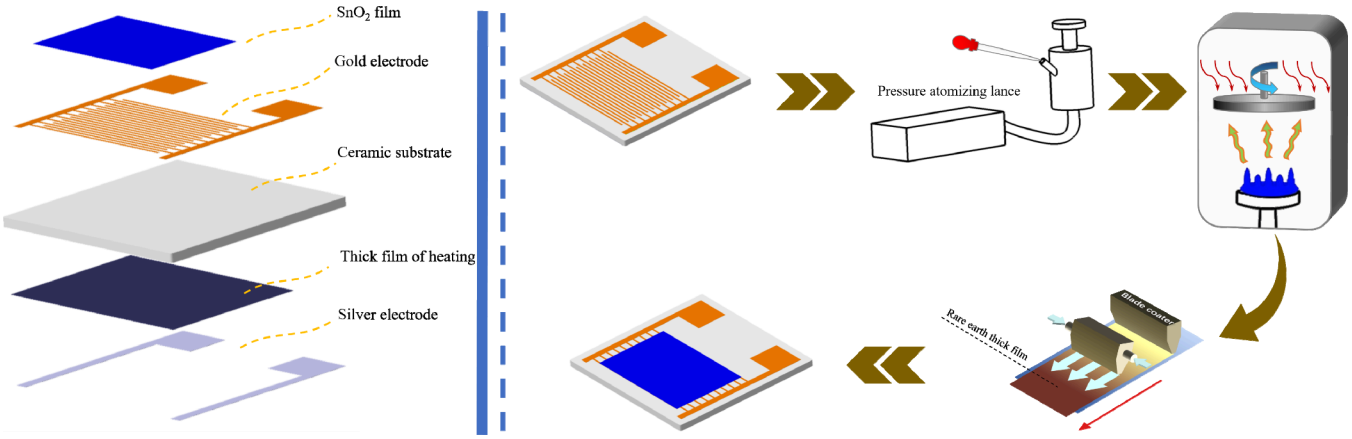

Figure 1. Schematic illustration of the understudy SnO_2 thin film sensor.

obtained sensors are commonly poor due to the need to use connectors in the sensor preparation process, resulting in it being difficult to promote industrial applications. Furthermore, the film layer of the sensor using connectors easily crumbles and falls off when exploited for a long time at high temperatures, which seriously affects the service life of the sensor. Therefore, the purpose of this context is to explore a convenient and fast sensor preparation method to reduce the sensor production cycle and improve sensor performance consistency and service life.

In the present work, the nanostructured SnO_2 thin films with broccoli-like structure nanoparticles are appropriately fabricated via convenient chemical deposition and subsequent heat treatment, and the detection performance of VOCs is systematically examined through the symbolization of resistance changes in air and target gas. The measurement results reveal that the nanostructured SnO_2 thin film sensors exhibit better selectivity, higher sensitivity, and excellent long-term stability for ethanol detection. In addition, density functional theory (DFT) is employed to further discuss the sensing mechanism in detail based on the change in electrical resistance of the sensor, and the calculated results agree well with those obtained from the experiment.

2. EXPERIMENTAL PROCEDURE

2.1. Materials. Stannic chloride pentahydrate ($SnCl_4 \cdot 5H_2O$, 99%) was purchased from Shanghai Aladdin Biochemical Technology Co., Ltd., xylene and isopropyl alcohol were prepared from Tianjin Fuyu Fine Chemical Co., Ltd., ethanol and acetone were purchased from Chengdu Jinshan Chemical Reagent Co., Ltd., and methanol, ethyl ether, and formaldehyde solution were prepared from Chongqing Jiangchuan Chemical Co., Ltd. All of the above chemicals were of analytical grade.

2.2. Preparation of SnO_2 Thin Films and Sensors, as well as Gas-Sensing Measurements. In this paper, an adjustable rotating plate and a lance nozzle were respectively added in the upper and lower parts of the muffle furnace and a special heating furnace was obtained for preparing the nanostructured SnO_2 thin film sensor. The spraying equipment photograph and structural diagram were illustrated in detail in Figure S1. The understudied nanostructured SnO_2 thin films were fabricated in the following steps. First, the precursor solution was prepared by dissolving 0.0285 mol of $SnCl_4 \cdot 5H_2O$ in 20 mL of deionized water and stirring magnetically for 30 min. Second, the gold finger electrode or the glass substrate was placed based on the alumina ceramic substrate on the rotating plate in a heating furnace oven at 593.15 K for 15 min. Then, a thin layer of nanostructured SnO_2 was deposited on the preheated gold finger electrode or glass substrate via an atomizing pressure lens, and the carrier gas pressure and sputtering time were set to 0.5 kg/cm^2 and 20 s, respectively (the film thickness can be adjusted by changing the spraying time). After that, the SnO_2-nanostructured thin films were thermally annealed in a muffle furnace at 773.15 K for 2 h. It is then naturally cooled to room temperature to yield nanostructured SnO_2 thin films.

Here, nanostructured SnO_2 thin films on a glass substrate were employed only to characterize the composition, morphology, and microstructure. Finally, a thick film of heating was coated on the back of the gold finger electrodes, maintaining a certain temperature during sensor aging and detection. The schematic illustration of the SnO_2 thin film sensor is provided in Figure 1.

To enhance the reliability and stability of the SnO_2 thin film sensor, the as-prepared sensors were placed on the sensor ager (AS-20, Elitetech Co., Beijing, China) and aged for 8 and 24 h at room temperature and 120 °C, respectively. The gas sensing performance of all sensors was methodically measured by a CGS-8 system supplied by Elitetech, Beijing, China, and the photographs of sensor and testing equipment are shown in Figure S2. In the present investigation, all measurement responses were defined as R_a/R_g, where R_a and R_g in order represent the resistance in air and the target gas.

2.3. Characterization. The composition and crystal structure of the samples were determined by using X-ray diffraction (XRD) and Raman spectra. XRD patterns were measured on a Rigaku D Max 2550 diffractometer using Cu Kα1 radiation (λ = 0.15406 nm) with a scanning speed of 5°/min in the 2θ range from 20 to 80°. Raman spectroscopy was also implemented to identify the compound with a LabRAM HRUV spectrometer. The morphology and microstructure of the samples were methodically examined using a field emission scanning electron microscope (SEM, USA FEI Nova Nano-SEM 230). X-ray photoelectron spectroscopy (XPS) was also performed on a Thermo Scientific K-Alpha spectrometer with an AlKα source. In addition, the binding energies were calibrated by taking the C 1s peak at 284.6 eV.

https://doi.org/10.1021/acsomega.3c09623
ACS Omega 2024, 9, 16055−16062

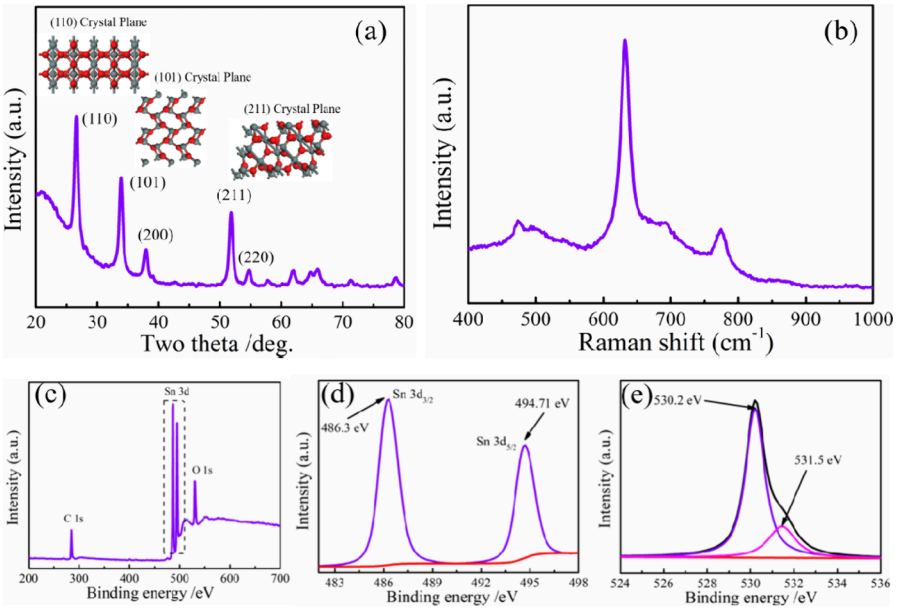

Figure 2. (a) XRD pattern. (b) Raman spectra. (c) XPS survey spectra for the nanostructured SnO_2 thin film. (d, e) High-resolution Sn 3d and O 1s spectra of the nanostructured SnO_2 thin film, respectively.

3. RESULTS AND DISCUSSION

3.1. Structure and Morphology Characterization. Herein, the crystalline structures and elemental compositions of the prepared SnO_2 nanostructured thin films were characterized by XRD and Raman spectroscopy, as presented in Figure 2a,b. All of the characteristic peaks in Figure 2a are completely consistent with the standard PDF cad SnO_2 (JCPDS No. 41-1445), and the diffraction peaks at 26.57, 33.87, 37.96, 51.80, and 54.73° correspond to (110), (101), (200), (211), and (220) of SnO_2 crystallite planes, respectively. Raman spectroscopy was further used to identify the crystalline structures and compositions of the as-prepared SnO_2 thin film, and three Raman peaks located at 473, 632, and 774 cm^{-1} could be identified for the nanostructured SnO_2 thin film (see Figure 2a). These identified peaks can be attributed to the Eg, A1g, and B2g modes of Sn−O symmetric vibration, respectively.[32] The XRD and Raman results clearly show the presence of a SnO_2 nanostructure.

In this work, XPS spectra were recorded to analyze the surface chemical bonding states of the as-prepared SnO_2 thin film. The XPS investigation presents the core-level spectra for C 1s, Sn, and 3d (Figure 2c). Obviously, the Sn 3d spectra exhibit two characteristic peaks located at 486.3 and 494.71 eV, as illustrated in Figure 2d, which can be attributed to the existence of Sn 3 $d_{3/2}$ and 3 $d_{5/2}$. This result is in good agreement with the Sn(IV) oxidation state of SnO_2. After calibration of O 1s spectra, the mixed characteristic peak of O 1s can be converted into two peaks (~530.2 and ~ 531.5 eV) with the Gaussian−Lorentzian line shape, as presented in Figure 2e. The peak located at ~530.2 eV originates from the oxygen atom in the SnO_2 lattice, and the peak at ~531.5 eV can be related to the absorbed H_2O and/or adsorbed oxygen on the surface of the SnO_2 thin film.

The morphology and configuration of the prepared SnO_2 thin film are first clarified by FESEM observation. The SnO_2 thin film sensors with different film thicknesses could be obtained by adjusting the sputtering time. In this paper, the film thickness with the maximum sensing response was obtained when the spraying time was 20 s, and the film thickness is about 2.8 μm (Figure S3). The low-magnification SEM image showed that the nanostructured SnO_2 thin film consisted of two different sizes of broccoli-like structure nanoparticles, as illustrated in Figure 3a. It can be seen in

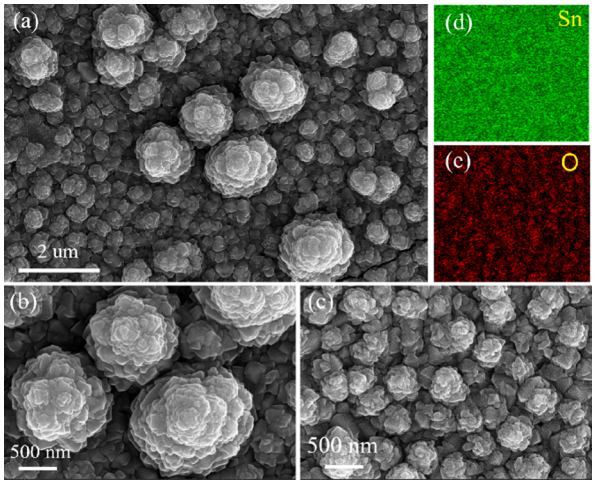

Figure 3. SEM images and elemental mapping of the nanostructured SnO_2 thin film: (a−c) SEM images. (d, e) Elemental mapping.

Figure 3b that the average diameter of large-size broccoli structure nanoparticles is about 900 nm and the average diameter of a small size is about 460 nm according to Figure 3c. In addition, the large- and small-sized broccoli-like structure SnO_2 nanoparticles exhibit good uniformity and morphological compatibility. The elemental mappings (Figure 3d,e) show the homogeneous spatial distributions of O and Sn, while being consistent with the structural characteristics of the SnO_2 broccoli nanoparticles.

3.2. Gas-Sensing Performance. The broccoli-like nanoparticles with multiple layered sheet-like structures not only exhibit a reasonable architecture to avoid the agglomeration of sheet-like structures between nanoparticles to maintain their

https://doi.org/10.1021/acsomega.3c09623
ACS Omega 2024, 9, 16055−16062

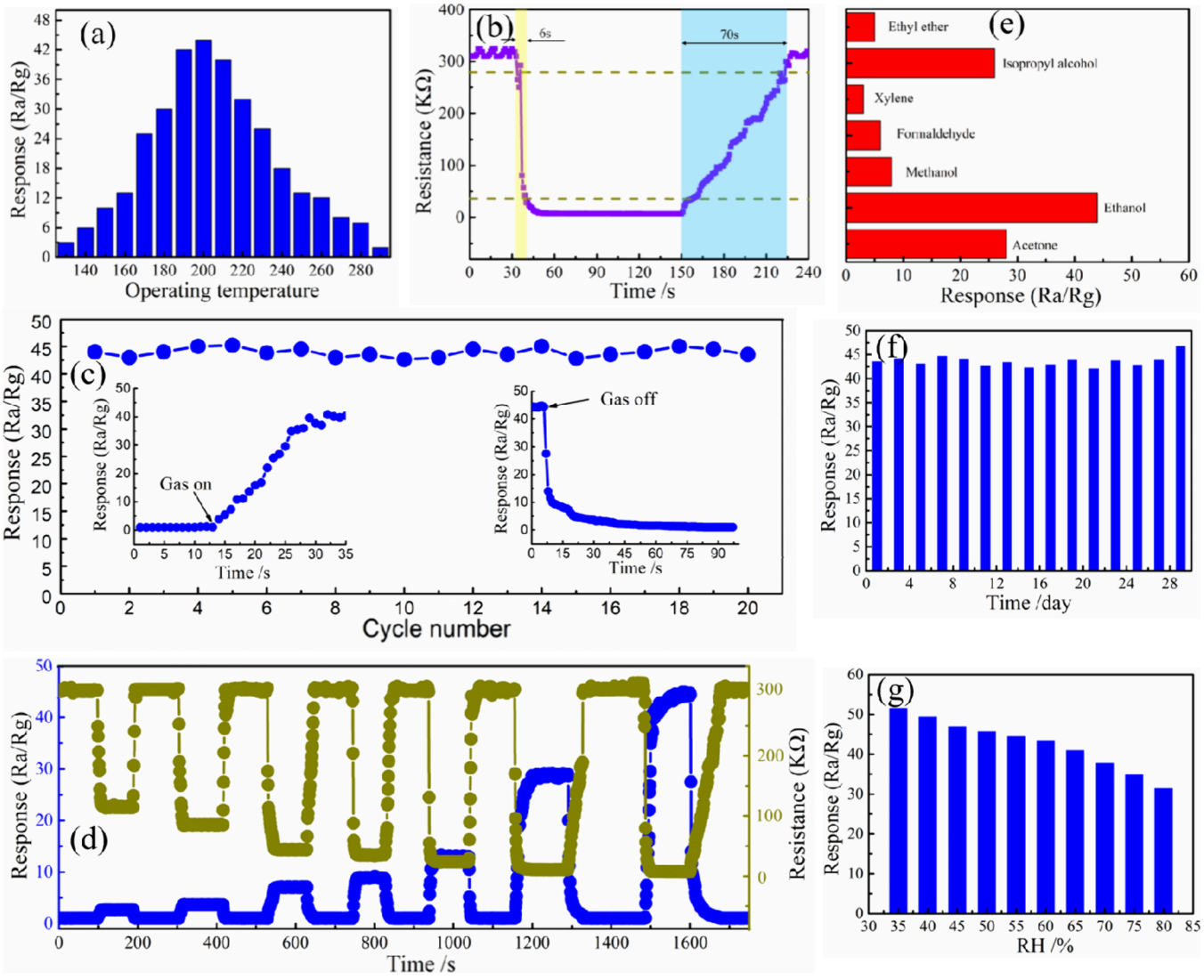

Figure 4. (a) Sensing response in terms of the operating temperature in 100 ppm of ethanol gas. (b) The response time and recovery time in 100 ppm of ethanol gas at 200 °C. (c) Sensing responses for 20 cycles in 100 ppm of ethanol gas at 200 °C. (d) Sensing responses in terms of the ethanol gas concentration in the 1−100 ppm range at 200 °C. (e) Selective responses to various target gases at 200 °C and 100 ppm exposure concentration. (f) Stability of the gas sensor in 100 ppm of ethanol vapor at 200 °C. (g) Sensing responses to various humidity levels in 100 ppm of ethanol vapor at 200 °C.

high-activated surfaces but also provide numerous gas contact areas to guarantee the fast gas diffusion and transport capability to reach or leave these surfaces. Therefore, the special nanostructure is considered as satisfying architecture with respect to the improvement of sensing performances. Herein, the CGS-8 system was implemented to measure the resistance changes when the SnO_2 thin film sensors were prepared toward air and target gas, and their sensing properties were methodically examined via the *Ra*/*Rg* definition method. The film thickness is critical to the sensing response of the SnO_2 thin film sensor, the maximum sensing response (~44) toward 100 ppm of ethanol gas was obtained when the spraying time was 20s (Figure S4), and the corresponding film thickness is about 2.8 μm.

In general, an appropriate operating temperature may improve the surface activity of the sensor, resulting in an enhanced sensing response and reduced recovery time. It can be clearly seen that the maximum response (~44) is obtained at an operating temperature of 200 °C compared to 100 ppm ethanol gas in Figure 4a, indicating that 200 °C is the optimal operating temperature for the nanostructured SnO_2 thin film. What is remarkable is that the response of the sensor for lowering the operating temperature to 150 °C is still more than 10, which indicates that the SnO_2 thin film sensor is still ideal for detecting combustible gases, especially ethanol gas.

In general, we can conclude that a higher adsorption energy may shorten the response time and increase the recovery time. We found that ethanol gas has large adsorption energy on the SnO_2 active crystal plane (Table 2). This fact fully explains why the response and recovery times were obtained as 6 and 70 s, respectively, from Figure 4b. In addition, cyclability was also examined to assess the reliability and repeatability of the developed SnO_2 thin film sensor. Continuous measurement of ethanol gas was also performed, as demonstrated in Figure 4c.

The typical sensing responses of the SnO_2 thin film sensor to several concentrations of ethanol gas at 200 °C were examined to analyze the dynamic and continuous response recovery behaviors, and the response results are shown in Figure 4d.

https://doi.org/10.1021/acsomega.3c09623
ACS Omega 2024, 9, 16055−16062

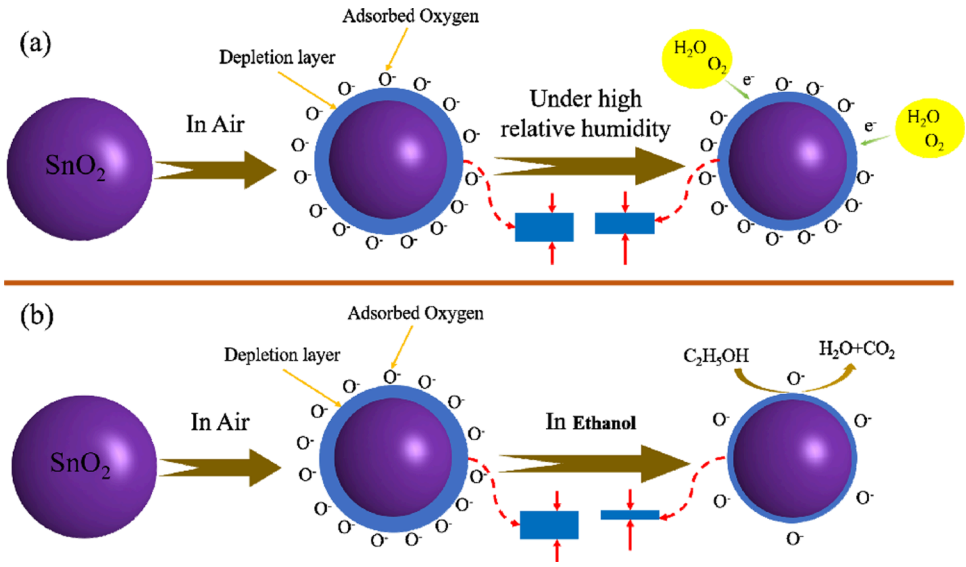

Figure 5. Schematic illustration of (a) the influence of the water molecules on the SnO_2 film sensor depletion layer under high relative humidity and (b) the ethanol gas sensing mechanism.

Table 1. Comparison between Gas Sensing Properties of Various Composites toward Ethanol

sensor material	concentration (ppm)	R_a/R_g	response/recovery time (s)	operating temperature (°C)	reference
SnO_2 microcubes	100	3	−/−	240	23
CeO_2-SnO_2 nanosheets	100	44	25/6	340	ref 34
SnO_2 CeO_2 nanofibers	200	55		370	ref 35
Fe_2O_3-SnO_2 nanoparticle-coated nanowire	200	57	−/−	300	ref 36
SnO_2 hollow fiber	500	48		260	ref 37
SnO_2 hierarchical nanostructure	100	32		275	ref 38
nanostructured SnO_2 thin film	100	44	6/70	200	present work

The plotted results reveal that the resistance and response curves of the sensor are regularly subjected to seven measurement cycles with increasing concentrations of ethanol gas from 1 to 100 ppm at 200 °C. The responses are approximately 2.7, 3.6, 7.0, 8.8, 13.1, 28, and 44 to 1, 2, 5, 10, 20, 50, and 100 ppm of ethanol gas. Furthermore, the ethanol sensor also presented a linear fitting curve from 1 to 100 ppm of ethanol gas at 200 °C with a slope of 0.415 ppm^{-1} (Figure S5). This helpful feature means that the circuit unit of the sensor can be made simpler, thus increasing the reliability and reducing operation cost.

In order to assess the limit of detection (LOD), 10 continuous monitoring cycles were conducted at a low concentration of 1 ppm (Figure S6). The mean of the 10 individual responses and the standard deviation of the noise level were ca. 2.64 and 0.102, respectively. Thus, the LOD was approximately evaluated to be 0.73 ppm based on a signal-to-noise ratio (S/N) of 3. The detailed calculation method is described in the Supporting Information. The results indicated that the sensor based on the thin film of nanostructured SnO_2 exhibits good reproducibility and sequential detection capabilities. Additionally, the selective responses of the SnO_2 thin film sensor toward different gases were estimated and the tested results were then plotted, as shown in Figure 4e. It can be clearly seen that the sensory responses are 44, 28, 26, 8, 6, 5, and 3 corresponding to 100 ppm ethanol, acetone, isopropyl alcohol, methanol, formaldehyde, ethyl ether, and xylene at 200 °C. Although the tested results show that the developed sensor based on nanostructured SnO_2 thin film exhibits excellent selectivity toward ethanol gas, it also illustrates that the sensor also presents cross-sensitivity to other gases other than ethanol. This is because other target gases will more or less reduce the number of negative oxygen ions on the sensor surface.

In this context, the long-term reproducibility of the SnO_2 thin film sensor toward 100 ppm ethanol gas at 200 °C during 30 days was performed with a 2-day interval measurement, as illustrated in Figure 4f. The obtained results reveal that the sensing response did not substantially alter with the passing of the test time, and they clearly show that the SnO_2 thin film sensor is capable of exhibiting good long-term stability. For the gas sensor, it is a very important indicator to evaluate the effect of ambient humidity (RH) due to the adsorption of water molecules, which could change the state of oxygen anions on the metal oxide surface. Therefore, the sensing responses to 100 ppm of ethanol gas were measured in the RH range from 35 to 80% at 200 °C, as shown in Figure 4f. It clearly evidences that the sensory response lessens with increasing RH. This is essentially attributed to the fact that the number of oxygen anions decreased with the increase in the number of water molecules adsorbed on the surface SnO_2 thin film sensor and thus the surface detection activity.[33] The influence of the water molecules on the SnO_2 film sensor depletion layer under high relative humidity is shown in Figure 5a.

As presented in 1, the sensing performances of detecting ethanol gas in our work were compared with those of previous investigations. From Table 1, the developed sensor based on nanostructured SnO_2 thin film shows a relatively higher sensing response and lower operating temperature than that reported in the literature.

https://doi.org/10.1021/acsomega.3c09623
ACS Omega 2024, 9, 16055−16062

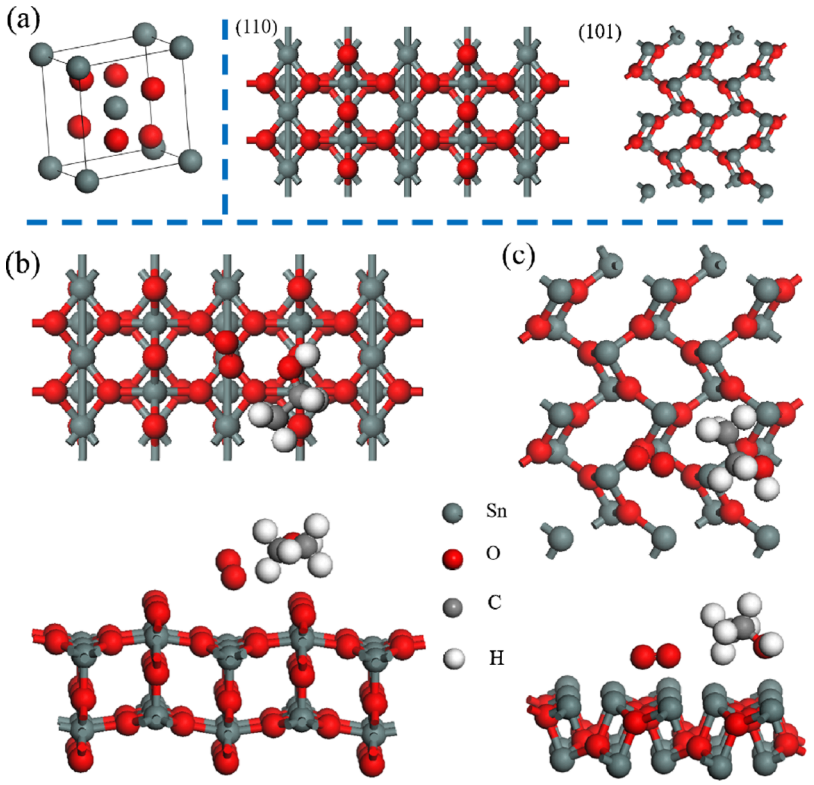

Figure 6. (a) The crystal structure of SnO_2 and the calculation models of two crystal planes. (b, c) The stable adsorption configurations of the oxygen and ethanol molecules on the (110) and (101) SnO_2 crystal planes, respectively.

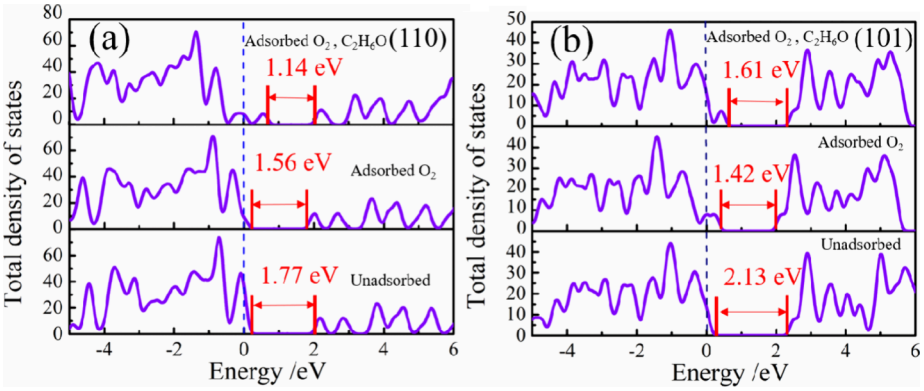

Figure 7. Density of states of the two crystalline planes, including unabsorbed, adsorbed O_2, and adsorbed both an O_2 and an ethanol: (a) (110) crystal plane; (b) (101) crystal plane.

3.3. Theoretical Calculations and Analyses. In this work, DFT is employed to evaluate the electronic properties and charge transfer when the SnO_2 thin film sensor adsorbs oxygen and ethanol gas, revealing the gas-sensing mechanism of the SnO_2 sensor.[38−42] The crystal planes (110) and (101) were employed as calculation models according to the optimal growth characteristics of SnO_2, and these two crystal planes exhibit obvious characteristic peaks in the XRD pattern. The details of the calculated models of pure SnO_2 and the stable adsorption configuration of oxygen and ethanol molecules are demonstrated in Figure 6, and the calculated results are provided in Figure 7.

It can be evidently seen that the band gaps of (110) and (101) crystal planes without adsorption are 1.77 and 2.13 eV, respectively, as illustrated in Figure 7. These calculated band gaps are all smaller than those obtained experimentally for SnO_2 (3.65 eV); this is because the generalized gradient approximation (GGA) method tends to underestimate the band gap. The band gap of (110) and (101) crystal planes decrease to 1.56 and 1.42 eV by adsorbing an oxygen molecule. Meanwhile, 0.12 and 0.16 e of (110) and (101) crystal planes are transferred to the oxygen adsorbent in 2, respectively. As a

Table 2. Charge Transfer and Adsorption Energy of the Three-Crystal Planes of SnO_2

	the charge transfer (e)		the adsorption energy (eV)	
crystal plane	adsorbed O_2	adsorbed C_2H_6O	adsorbed O_2	adsorbed C_2H_6O
(110)	−0.12	−0.16	−9.35	−25.37
(101)	−0.16	−0.18	−8.45	−23.93

https://doi.org/10.1021/acsomega.3c09623
ACS Omega 2024, 9, 16055−16062

result, the number of conducting electrons on the surface of the SnO_2 sensor decreases and the resistance of the sensor becomes high. The oxygen absorption energies of −9.35 and −8.45 eV correspond to (110) and (101) crystal planes, which indicates the stability of oxygen absorption of these two crystal planes. When the SnO_2 sensor is toward ethanol gas, the ethanol absorption energy values for (110) and (101) crystal planes are −25.37 and −23.93 eV, respectively. It is worth mentioning that the larger adsorption energy makes the adsorption rate faster and thus the response time becomes faster. On the contrary, it slows down the sensor recovery process and thus increases the sensor recovery time. This is why our test measured a response time of only 6 s and a recovery time of 70 s, as illustrated in Figure 4.

In addition, the absorbed ethanol molecules react with oxygen to produce carbon dioxide and water on the surface of the SnO_2 sensor; the schematic illustration of the ethanol gas sensing mechanism is shown in Figure 5b. As a result, the electrons transferred to the oxygen are then released to the SnO_2 sensor and the conductivity of the SnO_2 sensor is enhanced.[19] It is worth noting that the adsorption and desorption of oxygen and ethanol molecules are a dynamic equilibrium process. The adsorption of oxygen and ethanol molecules, which are not involved in the REDOX reaction, is also capable of altering the electronic structure of the sensor. Therefore, the band gap change is reduced from 1.77 and 2.13 eV to 1.14 and 1.61 eV from the calculated results in Figure 7, respectively.

4. CONCLUSIONS

SnO_2-nanostructured thin films were successfully fabricated using a suitable chemical deposition, and their sensory properties were systematically examined by symbolizing the R_a/R_g definition method. The morphology and microstructure suggested that the nanostructured SnO_2 thin layer consists of two dissimilar sizes of broccoli-like structure nanoparticles. The large-sized broccoli-like structure nanoparticles are mainly specified with a large size of about 900 nm and a small size of about 460 nm. The obtained results reveal that the achieved sensing response of the SnO_2 nanostructured sensor was about 44 times when it was toward 100 ppm of ethanol gas. In addition, the SnO_2-nanostructured sensor is very suitable for the detection of those flammable VOC gases due to obtaining a low operating temperature of 200 °C. The developed sensor offered high selectivity for ethanol gas and exhibited a fast-sensing speed. Additionally, the DFT was implemented to evaluate the electronic properties, and then the gas sensing mechanism of the nanostructured sensor based on the SnO_2 thin film was systematically explained.

■ ASSOCIATED CONTENT

Supporting Information

The Supporting Information is available free of charge at https://pubs.acs.org/doi/10.1021/acsomega.3c09623.

SnO_2 thin film sensor spraying equipment photograph and structural diagram; photograph of the sensor and testing equipment; SEM image of SnO_2 thin film thickness; function of the sensing responses and sputtering time; linear fitting curve of SnO_2 film sensor from 1 to 100 ppm at 200 °C; obtained 10 sensing responses of SnO_2 film sensor in 1 ppm ethanol gas at 200 °C; the stable adsorption configurations of the oxygen and ethanol molecules on the (110) SnO2 crystal planes; the stable adsorption configurations of the oxygen and ethanol molecules on the (101) SnO2 crystal planes; calculation method for LOD; and detailed parameters of theoretical calculation (PDF)

■ AUTHOR INFORMATION

Corresponding Author

Quan Xie − *College of Big Data and Information Engineering, Guizhou University, Guiyang 550025, China;* orcid.org/0000-0002-2848-1745; Email: qxie@gzu.edu.cn

Authors

Yu Zhang − *College of Big Data and Information Engineering, Guizhou University, Guiyang 550025, China*

Lin Lyu − *College of Big Data and Information Engineering, Guizhou University, Guiyang 550025, China*

Jiang Zou − *College of Big Data and Information Engineering, Guizhou University, Guiyang 550025, China*

Zhou Lu − *College of Big Data and Information Engineering, Guizhou University, Guiyang 550025, China*

Complete contact information is available at: https://pubs.acs.org/10.1021/acsomega.3c09623

Notes

The authors declare no competing financial interest.

■ ACKNOWLEDGMENTS

This work was financially supported by the National Natural Science Foundation of China (No. 51801039 and No. 61264004), Natural Science Foundation of Guizhou Province, China (No. [2020]1Y205, [2019] 1248), and High-level Creative Talent Training Program in Guizhou Province of China (Grant No. [2015]4015). The authors would like to express their gratitude to EditSprings (https://www.editsprings.cn) for the expert linguistic services provided.

■ REFERENCES

(1) Li, G.; Cheng, Z.; Xiang, Q.; Yan, L.; Wang, X.; Xu, J. Q. Biometal PdAu decorated SnO_2 nanosheets based gas sensor with temperature-dependent dual selectivity for detecting formaldehyde and acetone. *Sens. Actuators B Chem.* **2019**, *283*, 590−601.

(2) Shaalan, N. M.; Yamazaki, T.; Kikuta, T. Influence of morphology and structure geometry on NO_2 gas-sensing characteristics of SnO_2 nanostructures synthesized via a thermal evaporation method. *Sens. Actuators B* **2011**, *153*, 11−16.

(3) Shen, Y.; Yamazaki, T.; Liu, Z.; Jin, C.; Kikuta, T.; Nakatani, N. Porous SnO_2 sputtered flms with high H_2 sensitivity at low operation temperature. *Thin Solid Films* **2008**, *516*, 5111−5117.

(4) Tyagi, P.; Sharma, A.; Tomar, M.; Gupta, V. Metal oxide catalyst assisted SnO_2 thin film based SO_2 gas sensor. *Sens. Actuators B Chem.* **2016**, *224*, 282−289.

(5) Lyu, L.; Xie, Q.; Yang, Y. A novel CeO_2 Hollow-Shell sensor constructed for high sensitivity of acetone gas detection. *Appl. Surf. Sci.* **2022**, *571*, No. 151337, DOI: 10.1016/j.apsusc.2021.151337.

(6) Arun Kumar, K. L.; Durgajanani, S.; Jeyaprakash, B. G.; Balaguru Rayappan, J. B. Nanostructured ceria thin film for ethanol and trimethylamine sensing. *Sens. Actuators B* **2013**, *177*, 19−26.

(7) Umar, A.; Almas, T.; Ibrahim, A. A.; Kumar, R.; AlAssiri, M. S.; Baskoutas, S.; Akhtar, M. S. An efficient chemical sensor based on CeO_2 nanoparticles for the detection of acetylacetone chemical. *J. Electroanal. Chem.* **2020**, *864*, No. 114089.

(8) Van, D.; Nguyen, T. T. D.; Majhi, S. M. Ionic liquid-supported synthesis of CeO_2 nanoparticles and its enhanced ethanol gas sensing

https://doi.org/10.1021/acsomega.3c09623
ACS Omega 2024, 9, 16055−16062

properties. *Mater. Chem. Phys.* **2019**, 1 DOI: 10.1016/j.matchemphys.2019.03.025.
(9) Singh, I.; Dey, S.; Santra, S.; Landfester, K.; Muñoz-Espí, R.; Chandra, A. Cerium-doped copper (II) oxide hollow nanostructures as efcient and tunable sensors for volatile organic compounds. *ACS Omega* **2018**, *3*, 5029−5037.
(10) Xue, X. Y.; Xing, L.; Chen, Y. J.; Shi, S. L.; Wang, Y. G.; Wang, T. H. Synthesis and H_2S sensing properties of CuO-SnO_2 core/shell P-N junction nanorods. *J. Phys. Chem. C* **2008**, *112*, 12157−12160.
(11) Tang, W.; Wang, J.; Yao, P.; Li, X. Hollow hierarchical SnO_2−ZnO composite nanofbers with heterostructure based on electrospinning method for detecting methanol. *Sens. Actuators B Chem.* **2014**, *192*, 543−549.
(12) Gawali, S. R.; Patil, V. L.; Deonikar, V. G.; Patil, S. S.; Patil, D. R.; Patil, P. S.; Pant, J. Ce doped NiO nanoparticles as selective NO_2 gas sensor. *J. Phys. Chem. Solids* **2018**, *114*, 28−35.
(13) Mehta, S.; Nadargi, D.; Tamboli, M.; Patil, V.; Mulla, I.; Suryavanshi, S. Macroporous WO_3: tunable morphology as a function of glycine concentration and its excellent acetone sensing performance. *Ceram. Int.* **2019**, *45*, 409−414.
(14) Righettoni, M.; Tricoli, A.; Pratsinis, S. E. Si: WO_3 sensors for highly selective detection of acetone for easy diagnosis of diabetes by breath analysis. *Anal. Chem.* **2010**, *82*, 3581−3587.
(15) Shen, J. Y.; Wang, M. D.; Wang, Y. F.; Hu, J. Y.; Zhu, Y.; Zhang, Y. X.; Li, Z. J.; Yao, H. C. Iron and carbon codoped WO_3 with hierarchical walnutlike microstructure for highly sensitive and selective acetone sensor. *Sens. Actuators B* **2018**, *256*, 27−37.
(16) Jayababu, N.; Poloju, M.; Shruthi, J.; Reddy, M. V. R. Ultrasensitive resistivity-based ethanol sensor based on the use of CeO_2-Fe_2O_3 core-shell microclusters. *Microchim. Acta* **2019**, 712.
(17) Wang, M. Y.; Zhu, Y. Y.; Meng, D.; Wang, K. K.; Wang, C. Y. A novel room temperature ethanol gas sensor based on 3D hierarchical flower-like TiO2 microstructures. *Mater. Lett.* **2020**, *277*, No. 128372.
(18) Raghu, A. V.; Karuppanan, K. K.; Nampoothiri, J.; Pullithadathil, B. Flexible ethanol gas sensor based on TiO2 nanoparticles-grafted 2D-titanium carbide nanosheets. *ACS Appl. Nano Mater.* **2019**, *2*, 1152−1163.
(19) Jayababu, N.; Poloju, M.; Shruthi, J.; Reddy, M. V. R. Semi shield driven p-n heterostructures and their role in enhancing the room temperature ethanol gas sensing performance of NiO/SnO2 nanocomposites. *Ceram. Int.* **2019**, *45*, 15134−15142.
(20) Dwivedi, P.; Das, S.; Dhanekar, S. Wafer-scale synthesized MoS2/Porous Silicon nanostructures for efficient and selective ethanol sensing at room temperature. *Acs Appl. Mater. Interfaces* **2017**, *9*, 21017−21024.
(21) Park, S.; Kim, S.; Sun, G. J.; Lee, C. Synthesis, Structure, and Ethanol Gas Sensing Properties of In_2O_3 Nanorods Decorated with Bi_2O_3 Nanoparticles. *ACS Appl. Mater. Interfaces* **2015**, *7*, 8136−8146.
(22) Zhu, L.; Zeng, W.; Li, Y. A non-oxygen adsorption mechanism for hydrogen detection of nanostructured SnO_2 based sensors. *Mater. Res. Bull.* **2019**, *109*, 108−116.
(23) Huang, J.; Xu, X.; Gu, C.; Wang, W.; Geng, B.; Sun, Y.; Liu, J. Effective VOCs gas sensor based on porous SnO_2 microcubes prepared via spontaneous phase segregation. *Sens. Actuators B Chem.* **2012**, *173*, 599−606.
(24) Korotcenkov, G.; Cho, B. K. Instability of metal oxide-based conductometric gas sensors and approaches to stability improvement. *Sens. Actuators B Chem.* **2011**, *156*, 527−538.
(25) Waitz, T.; Becker, B.; Wagner, T.; Sauerwald, T.; Kohl, C. D.; Tiemann, M. Ordered nanoporous SnO_2 gas sensors with high thermal stability. *Sens. Actuators B* **2010**, *150*, 788−793.
(26) Wang, Y.; Zeng, Y.; Wang, L.; Lou, Z.; Qiao, L.; Tian, H.; Zheng, W. Ultrathin nanorod-assembled SnO_2 hollow cubes for high sensitive n-butanol detection. *Sens. Actuators B* **2019**, *283*, 693−704.
(27) Tonezzer, M.; Hieu, N. V. Size-dependent response of single-nanowire gas sensors. *Sens. Actuators B Chem.* **2012**, *163*, 146−152.
(28) Pavelko, R. G.; Vasiliev, A. A.; Llobet, E.; Vilanova, X.; Barrabés, N.; Medina, F.; Sevastyanov, V. G. Comparative study of nanocrystalline SnO_2 materials for gas sensor application: thermal stability and catalytic activity. *Sens. Actuators B* **2009**, *137*, 637−643.
(29) Liewhiran, C.; Tamaekong, N.; Wisitsoraat, A.; Phanichphant, S. Highly selective environmental sensors based on flame-spray-made SnO_2 nanoparticles. *Sens. Actuators B Chem.* **2012**, *163*, 51−60.
(30) Han, X. M.; Zhang, B.; Guan, S. K.; Liu, J. D.; Zhang, X.; Chen, R. F. Gas-sensing properties of SnO_2 nanobelts synthesized by thermal evaporation of Sn foil. *J. Alloys Compd.* **2008**, *461*, L26−L28.
(31) Wang, G. X.; Park, J. S.; Park, M. S.; Gou, X. L. Synthesis and high gas sensitivity of tin oxide nanotubes. *Sens. Actuators B Chem.* **2008**, *131*, 313−317.
(32) Ganesh, V.; Arif, M.; Manthrammel, M. A.; Shkir, M.; Singh, A.; Alfaify, S. Effect of La Doping on Key Characteristics of SnO_2 Thin Films Facilely Fabricated by Spin Coating Technique. *Opt. Mater.* **2019**, *94*, 277−285.
(33) Zito, C. A.; Perfecto, T. M.; Dippel, A. C.; Volanti, D. P.; Koziej, D. Low-temperature carbon dioxide gas sensor based on yolk−shell ceria nanospheres. *ACS. Appl. Mater. Inter.* **2020**, *12*, 17757−17763.
(34) Yan, S.; Liang, X.; Song, H.; Ma, S.; Lu, Y. Synthesis of Porous CeO_2-SnO_2 Nanosheets Gas Sensors with Enhanced Sensitivity. *Ceram. Int.* **2018**, *44*, 358−363.
(35) Qin, W. F.; Xu, L.; Song, J.; Xing, R.; Song, H. Highly Enhanced Gas Sensing Properties of Porous SnO_2-CeO_2 Composite Nanofibers Prepared by Electrospinning. *Sens. Actuators B Chem.* **2013**, *185*, 231−237.
(36) Choi, K. S.; Park, S.; Chang, S. P. Enhanced Ethanol Sensing Properties Based on SnO_2 nanowires Coated with Fe_2O_3 Nanoparticles. *Sens. Actuators B Chem.* **2017**, *238*, 871−879.
(37) Cao, J.; Zhang, T.; Li, F.; Yang, H.; Liu, S. Enhanced ethanol sensing of SnO_2 hollow micro/nanofibers fabricated by coaxial electrospinning. *New J. Chem.* **2013**, *37*, 2031−2036.
(38) Liu, Q.; Zhang, Z.; Li, W.; Xu, K.; Zou, R.; Hu, J. Ethanol gas sensor based on a self-supporting hierarchical SnO_2 nanorods array. *Cryst. Eng. Comm.* **2015**, *17*, 1800−1804.
(39) He, Y.; Li, D.; Gao, W.; Yin, H.; Chen, F.; Sun, Y. F. High-performance NO_2 sensors based on spontaneously functionalized hexagonal boron nitride nanosheets via chemical exfoliation. *Nanoscale* **2019**, *11*, 21909−21916.
(40) Beheshtian, J.; Peyghan, A. A.; Bagheri, Z. Detection of phosgene by Sc-doped BN nanotubes: A DFT study. *Sens. Actuators B Chem.* **2012**, *171*−*172*, 846−852.
(41) He, X.; Gui, Y. G.; Liu, K.; Xu, L. N. Comparison of sensing and electronic properties of C_2H_2 on different transition metal oxide nanoparticles (Fe_2O_3, NiO, TiO_2) modified BNNT (10, 0). *Appl. Surf. Sci.* **2020**, *521*, No. 146463.
(42) Segall, M. D.; Lindan, P. J. D.; Probert, M. J.; Pickard, C. J.; Hasnip, P. J.; Clark, S. J.; Payne, M. C. First-principles simulation: Ideas, illustrations and the CASTEP Code. *J. Phys. Condens. Mat.* **2002**, *14*, 2717−2744.

https://doi.org/10.1021/acsomega.3c09623
ACS Omega 2024, 9, 16055−16062